The Posterior Part of the Ventral Medial Nucleus of the Thalamus (or VMpo) Across Primates

Alternate series of coronal sections from the thalami of cynomolgus and rhesus macaques, pygmy chimpanzee, gibbon, orangutan, gorilla, and human were cyt at 50 um and stained for Nissl substance (thionin) and for calbindin 28kD (Novocastra). All brains except those of macaques and humans were obtained from Prof C.C. Sherwood and Prof P.R. Hof. Support for the use of the exotic primate brains was provided by the National Chimpanzee Brain Resource (NINDS grant NS092988). The bonobo measurements were obtained from slides in the laboratory of Prof. K. Semendeferi. As can be seen in the **Figure 1S** below, VMpo (*black arrows*) can be recognized cytoarchitectonically in all anthropoid primates, and in all it co-localizes with a region of dense, patchy staining for calbindin-positive terminal fibers throughout its postero-anterior extent (**Figure 1S, lower image**). The three-dimensional volume of VMpo was obtained in each case by outlining it in each alternate section using a camera lucida at 14x and then tracing the drawn outlines on a digitizing tablet for quantification. Corresponding measurements for each case and statistics are shown in **Table1S**. The quantitative (or 'allometric'; (1)) analysis indicated that the VMpo increased in size and complexity across this phylogenetic series. The graphs below (**Figure 2S**) demonstrate such size increase against total brain volume (top) and in relation to the volume of the ventral posterior (VP) nucleus of the thalamus (bottom). The results of the statistical interspecies regression analyses (stated in the lower right corner of each graph) show that the ratio of the volume of VMpo to the volume of VP has an exponent significantly greater than one ('hyperallometric'), consistent with the observed increase in size and complexity across this phylogenetic series of anthropoid primates. Although these observations are based on a limited number of samples, they suggest that VMpo enlarged during human evolution consistent with the view that it provided an important energetic advantage that underpinned the emergence of emotional or 'homeostatic' sentience (2). (The gibbon was omitted from the graphs because its brain volume was unavailable.)

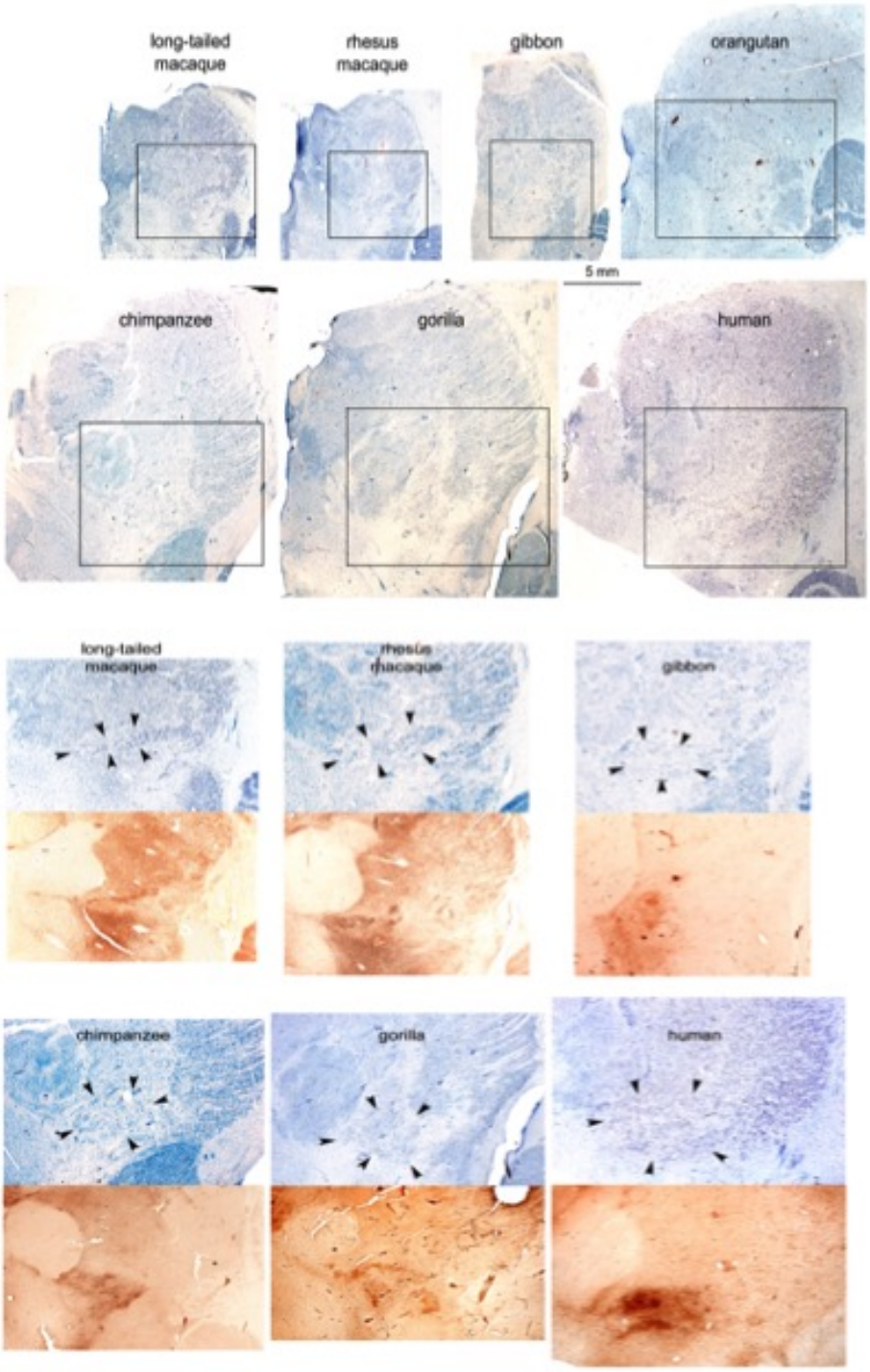

Figure 1S: The Posterior Part of the Ventral Medial Nucleus of the Thalamus (or VMpo) Across Primates. The boxed regions in the upper photomicrographs (which are all shown at the same magnification) are shown in the lower panel at higher power (the first three at twice the magnification of the others), together with an adjacent section stained for calbindin. The arrowheads outline the borders of VMpo, which can be differentiated from its neighbors both cytoarchitectonically and by the moderately dense clusters of calbindin-positive terminations in each primate's thalamus.

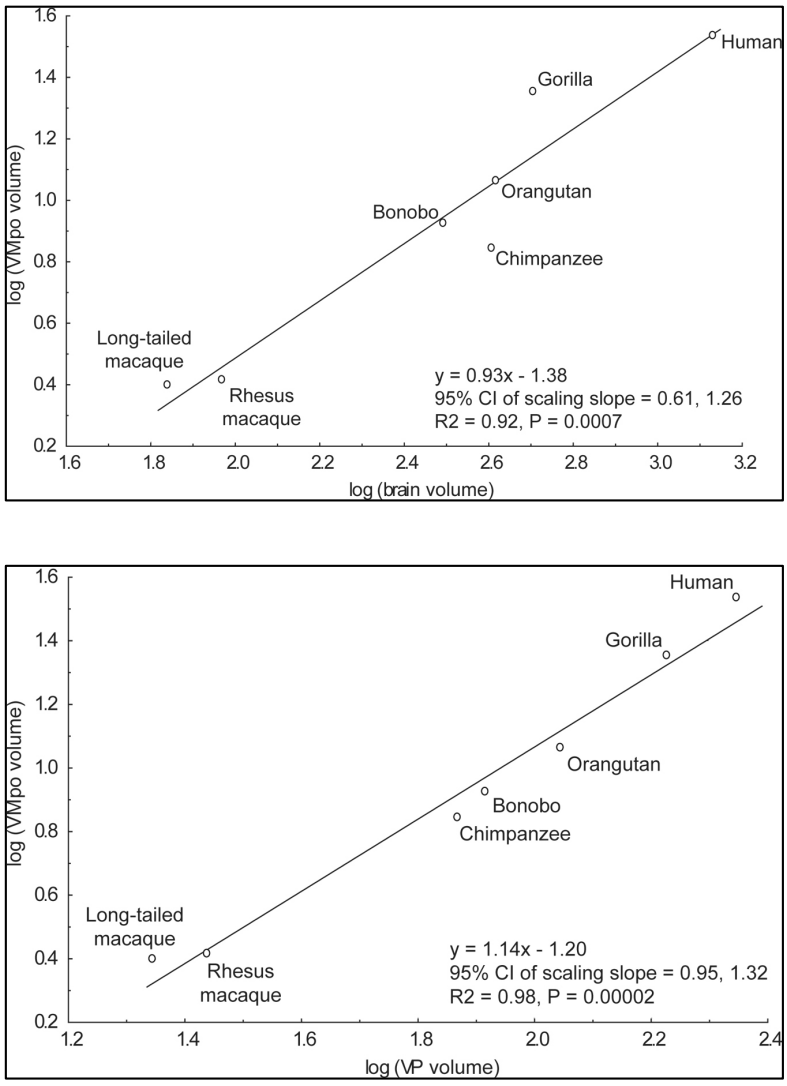

Figure 2S: Log plots of VMpo volume across primates. Size increase against total brain volume (top) and in relation to the volume of the ventral posterior (VP) nucleus of the thalamus (bottom) is shown. The results of the statistical interspecies regression analyses (lower right corner of each graph) show that the ratio of the volume of VMpo to the volume of VP has an exponent significantly greater than one ('hyperallometric').

Table 1S: Allometric Comparison of VMpo nucleus across primates				
	Case	VMpo Volume mm^3	VP Volume mm^3	VMpo/VP %
Long-Tailed	M123	2.96	26.44	11.2
	M125	2.45	18.40	13.3
	M155	2.11	21.37	9.9
Rhesus	Rh1	2.49	34.64	7.2
	M164R	2.26	21.37	10.6
	M170R	3.04	26.26	11.6
Gibbon	Mel-L	2.39	51.30	4.7
Orang	Orang1	6.95	112.40	6.2
	Thelma	16.20	108.87	14.9
Gorilla	Gor-1	19.17	113.08	17.0
	YN82-140	14.58	94.24	15.5
	Sylvia-L	33.80	298.88	11.3
	-R	30.76	266.11	11.6
Chimpanzee	Ch2	9.18	107.84	8.5
	Ch3	5.22	50.27	10.4
	Ch4	6.53	63.00	10.4
Bonobo	Zahlie	10.87	99.10	11.0
	YN86-137-R	8.42	82.38	10.2
Human	H8r	29.91	196.49	15.2
	SN207	38.73	247.64	15.6
	Mu-85-64	16.5	113.0	14.6
	Mu-109-66	23.4	176.1	13.3
	Mu-95-65	13.7	89.1	15.4
	Mu-90-65	21.0	100.4	20.9

IS THERE A DIRECT VAGAL-ACTIVATED PROJECTION TO INTEROCEPTIVE CORTEX?

METHODS

Electrophysiological recordings were performed in 16 Nembutal-anesthetized long-tailed (cynomolgus) macaque monkeys (Macaca fascicularis), as described in prior papers (3). In nine cases, electrical stimulation of the left and right vagus nerves was used as a guide in collaboration with S.I. Ito (Kumamoto Univ. Sch. Med., Japan). In the remaining eight cases, double- and triple-labeled connections were examined using fluorescent anterograde tracers injected at microelectrode recording sites in the thalamus (**Figure 3S**). Briefly, both left and right vagus nerves were isolated bilaterally in the neck and electrically stimulated (2 pulses at 200 Hz, 0.5 ms duration). The intensity (ca. 4mA) was ~10times greater than the threshold for suppression of spontaneous breathing with a 2 sec stimulus train at 50 Hz. Recordings of vagal-evoked potentials (VEPs) were obtained during microelectrode penetrations in the thalamus, in order to identify the response foci in VMb. Multiunit activity in relation to respiration or heart beat, or in response to taste, orofacial, or electrical vagus stimulation was examined. A glass micropipette was stereotaxically inserted at a VEP focus in VMb and wheat germ agglutinin conjugated to HRP (WGA*HRP) or fluorescent dextran was injected iontophoretically or hydraulically. After two to three weeks survival, the monkeys were perfused with fixative and the brain was cut in 50 µm sections in the coronal plane and examined (**Figure 3S**).

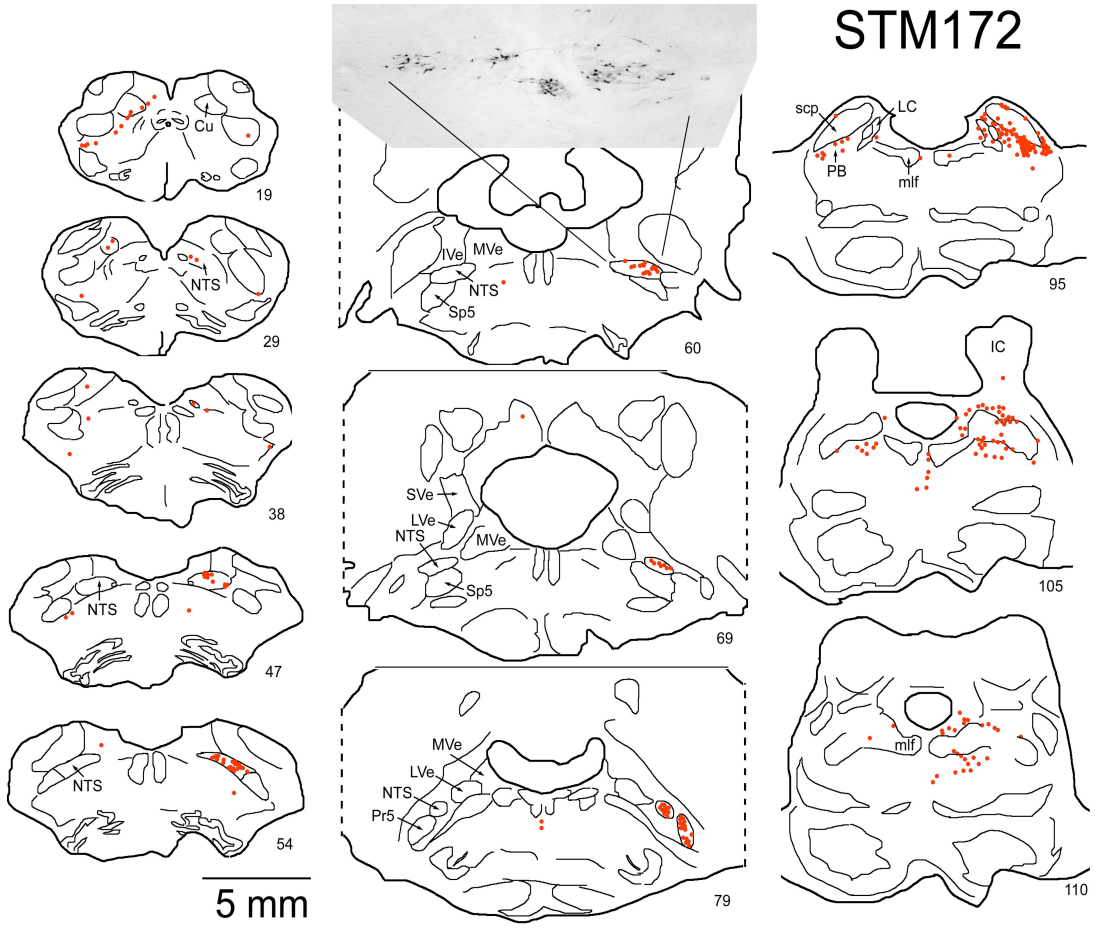

Figure 3S: Input to the thalamus from the NTS The brainstem origin of vagus-activated input to VMb in the macaque monkey was investigated using fluorescent dextrans, WGA*HRP, or biotinylated dextran amine for retrograde (and anterograde) labeling. As can be seen, labeled cell bodies were found consistently in the parabrachial nucleus (PB) and the nucleus of the solitary tract (NST) mainly ipsilaterally. Dense neuronal labeling was present in the anterior (gustatory) third of the NST, with modest labeling of neurons in the middle third and sparse labeling in the caudal third, both of which receive direct vagal input. Only a few cells were labeled in the reticular formation. Each red dot represents one labeled cell, and each level shown depicts all labeled cells observed in one section. Adapted from Ito S-I and Craig AD (Bud). Afferent projections to the vagus-responsive region of the thalamic parafascicular nucleus in monkeys. Society for Neuroscience 2007; Online planner 417.11 and Ito S-I and Craig AD (Bud). Afferent projections to the vagus-responsive 'associative' territory of the striatum. Society for Neuroscience 2006. Online planner 166.9.

DOES BREATHING FACILITATE ASYMMETRIC EMOTIONAL PROCESSING?

METHODS:

SUBJECTS:

Fifteen healthy subjects (6 males, 9 females) with an average age of 23.1 years (range 19-27) and an average education level of 13.4 years (range 13-15) gave written consent to participate in this study, which was approved by the University of California San Diego Human Research Protection Program. Subjects performed a paced breathing task described below designed to examine the effects of controlled slow breathing on brain activity associated with emotional processing.

BREATHING TASK DESIGN

Subjects performed a paced breathing task (**Figure 4S)** designed to examine the effects of controlled slow breathing on brain activity associated with emotional processing. Specifically, individuals were asked to synchronize their respiratory frequency to a continuous audio signal of the breath of a professional yoga instructor performing a slow breathing exercise. The audio recording of one breath was digitally modulated (by changing the wavelength of a single breath recording without changing the pitch or the amplitude) to construct slow and fast breathing epochs with inspiratory and expiratory phases of equal duration. Subjects were familiarized with the paradigm prior to entering the scanner room, instructed to use abdominal breathing, to breathe through their nose (to allow for measurement of each breath through the nasal canula), and to inhale and exhale so as to match the audio signal presented through the headphones. Resting respiratory rates of 10-20 cycles per minute are considered normal, whereas rates of 1-2 cycles per minute can only be achieved with advanced yoga and meditation training (4). The slow breathing rate in this study was set at 5 breaths/min, and the fast breathing rate was set at 20 breaths/min. These rates were tested during pilot studies in a separate group of subjects and were well tolerated. All subjects were novices to controlled breathing exercises.

During different breathing epochs, the subjects were presented with images from the International Affective Picture Set (IAPS) that had either positive (norm ratings 7.38 ± 1.47) or negative (norm ratings 2.27 ± 1.42) valence. Visual stimuli were projected onto a screen by the LCD monitor. Subjects were asked to only passively view the images.

Our paradigm had two breathing frequencies and two emotional valences, which resulted in four conditions: FAST/POSITIVE, FAST/NEGATIVE, SLOW/POSITIVE and SLOW/NEGATIVE. The presentation order of each condition was pseudo-randomized. Each epoch was presented for 36 sec and was interleaved with brief (6 sec) transition periods of one breath with a breathing frequency of 10 breaths/min. In addition, a short instruction period (2 breaths for fast and 1 breath for slow breathing epochs) preceded each breathing condition in order to induce the desired breathing state before emotional image presentation. The total duration of the task was 618 sec. Before scanning, the subjects were familiarized with the breathing task and were asked to practice a short, modified version. During the breathing practice, the subjects were not shown any positively or negatively valenced images.

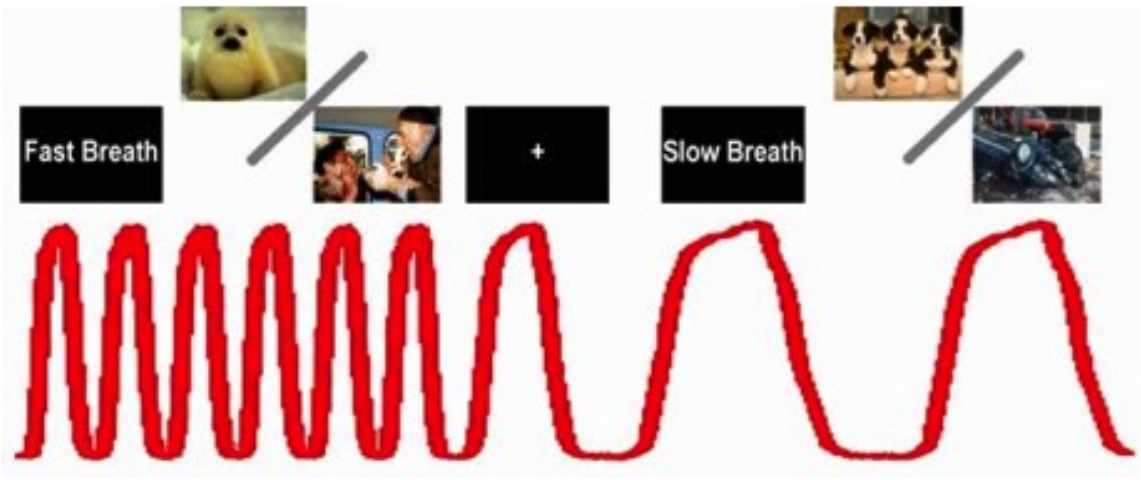

Figure 4S: Task Design. Fast (20 breaths/min) and slow (5 breaths/min) breathing epochs were presented in random order and controlled by the continuous audio signal (red). Subjects were instructed to passively view positive and negative images. Positive and negative images were presented during both slow and fast breathing allowing for examination of emotion x breathing rate interaction

AUTONOMIC MONITORING

Pulse (pulse oximetry; measured using a finger cuff placed on the left hand) and end-tidal CO_2 (EtCO2; measured using a nasal canula) were continuously measured during each functional run for each subject with an MRI-compatible InVivo physiological monitoring device (InVivo Magnitude TM 3150M MRI patient monitor, acquisition rate 40 Hz).

The pulse signal was analyzed for heart rate and for heart rate variability (HRV) with HRV analysis software package (5) and according to the guidelines laid down by the Task force of European Society of Cardiology and North American Society of Pacing and Electrophysiology (Task Force Guidelines 1996) (6). Briefly, the inter-beat-interval (IBI) values were visually inspected and potential artifacts due to missing or false heart rhythms, poor conductivity, etc. were manually removed. A low correction threshold was chosen for artifact correction in order to not to distort natural variability. In order to estimate parasympathetic activity during slow and fast controlled breathing, the HRV was analyzed in the time using one of the simplest time-domain variables, the standard deviation of the RR interval (SDNN). SDNN reflects all of the cyclic components responsible for variability in the period of recording in milliseconds, and it provides a valid estimate of the HRV (Task Force Guidelines 1996). We computed SDNN for each 36-sec-long slow and fast breathing epoch, and we compared the average SDNN for slow and fast breathing using a paired t-test.

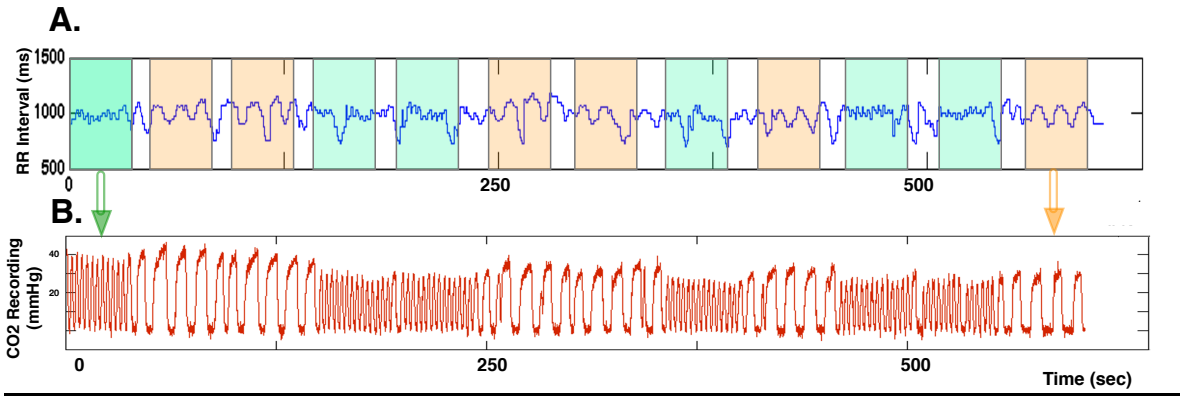

Figure 5S: Time-Domain Heart Rate Variability during Slow and Fast Breathing. An example subject's heart rate (RR interval) **(A)** and respiratory (CO2) **(B)** signals are shown for the entire breathing paradigm. Green – fast breathing epoch; Orange – slow breathing epoch.

IMAGE ACQUISITION

During the task, an fMRI run sensitive to blood oxygenation level-dependent (BOLD) contrast was collected for each subject using a 3.0 Tesla GE scanner (T2 * weighted echo planar imaging, TR = 2000 ms, TE = 32 ms, 64 x 64 matrix, 30 2.6-mm axial slices (1.4 mm gap), 309 scans; voxel size 3.4x3.4x4mm^3). fMRI acquisitions were time-locked to the onset of each trial. During the same experimental session for each subject, a high resolution T1-weighted image (FSPGR, TR = 11.4 ms, TE = 4.4 ms, TI=450 ms, flip angle = 12°, FOV = 250 x 250, 256x256 matrix, 172 1 mm slices) was obtained for anatomical reference.

IMAGING ANALYSIS

Imaging data were preprocessed and analyzed with the Analysis of Functional NeuroImages (AFNI) software package (7). Briefly, preprocessed time series data for each individual were analyzed using a multiple regression model corrected for autocorrelation consisting of four regressors of interest (fast/positive, fast/negative, slow/positive and slow/negative). In addition, nine regressors were entered into the linear regression model to account for variance of the BOLD signal that was not related to the neural control of breathing or emotion-related processes. Specifically, two regressors were used to account for instruction times and three for residual motion (in the roll, pitch, and yaw direction), and each individual's breathing and heart rate tracings were used to account for any periodic effects of breathing and heart-rate on the BOLD signal. Finally, two regressors for baseline and linear trends were used to eliminate slow signal drifts. A Gaussian filter with full width- half maximum 4 mm was applied to the voxel-wise percent signal change data to account for individual variations in the anatomical landmarks. Data from each subject were normalized to Talairach coordinates (8).

In order to ensure that movement induced by different breathing rates did not influence our findings, we compared motion parameters between the two types of breathing. Motion parameters were obtained from AFNI program 3dvolreg, which is motion-correction algorithm for aligning 3D volumes that assumes a rigid movement of the entire volume; it estimates 6 parameters for motion correction: Shifts along x-, y-, and z-axes; Rotations about x-, y-, and z-axes. We found no significant differences in any of the

six motion parameters (see **Table 2S** below). The overall motion for slow and fast breathing epochs was within the values suggested by the imaging community (e.g., AFNI) (i.e., <0.3mm for shifts and <0.3 degrees for ration).

Table 2S: Motion Parameters during Slow and Fast Breathing

Motion	SLOW	FAST	P-val
roll	0.07±0.05	0.07±0.06	0.98
pitch	-0.03±0.1	-0.04±0.11	0.57
yaw	-0.1±0.08	-0.08±0.08	0.23
dS	0.06±0.15	0.05±0.15	0.88
dL	0.02±0.02	0.02±0.03	0.61
dP	0.09±0.04	0.1±0.04	0.61

roll = rotation about the I-S axis; pitch = rotation about the R-L axis;
yaw = rotation about the AP axis (degrees);
dS = displacement in the Superior direction;
dL = displacement in the Left direction; dP = displacement in the Posterior direction (mm)

The following linear contrasts were examined: 1) [(Slow/Positive – Slow/Negative)] to see the relationship between slow breathing and emotional valence (reported in the main text); 2) [Fast/Negative – Fast/Positive)] to see the relationship between fast breathing and emotional valence (reported in the main text); and 3) [(Slow/Positive + Fast/Positive)]-[(Slow/Negative+Fast/Negative)] to examine main effects of emotional valence (reported below). Region of interest (ROI) masks were used for the bilateral insula and anterior cingulate cortices. Regions were based on atlases available in AFNI. Voxel-wise percent signal change data for the ROIs were entered into a t-test to examine activation during the above linear contrasts. Data for each ROI was thresholded based on Monte-Carlo simulations to guard against identifying false positive areas of activation(9). A priori voxel-wise probability of $p< 0.05$ and a-posteriori probability of $p<0.05$ for the cluster was used for each ROI. A Monte Carlo simulation (iterations =10,000) using AlphaSim was used to determine that for a search volume within the ROI a cluster size of 320mm^3 (5 voxels) was required to control for multiple comparisons maintaining an alpha of 0.05. The cluster t-values were calculated by averaging the voxel based t-values in each ROI. The average percent signal difference was extracted from regions of activation that were found to survive this threshold/cluster method and the average of the surviving voxels within the cluster was correlated with HRV indices.

RESULTS

TASK COMPLIANCE

All fifteen subjects completed the task in the scanner. In order to quantify each subject's performance on the task, the average breathing rate during each slow and fast breathing epoch was computed for each subject from the individual $EtCO_2$ trace and correlated with the expected breathing rate during each epoch. Subjects' breathing rates showed nearly perfect correlation with the expected breathing rates during the task (mean ± SEM: $r=0.995\pm0.03$, $p < 0.01$). This supports the conclusion that each subject performed the task adequately.

SUBJECTIVE EXPERIENCE

Post-test questionnaires obtained after the imaging session revealed that subjects found the task “interesting” (mean±SD: 3.1±0.8, 1 = not interesting, 4 = very interesting), reported feeling “relaxed” during the task (mean±SD: 3.5±1.2, 1 = very tense, 5 = very relaxed), and paid attention to the task (mean±SD: 3.5±0.5, 1 = very little; 4 = very much). Twelve out of fifteen subjects could easily “keep pace” with the breathing stimulus, but eight of them reported that slow breathing was more difficult than fast breathing. All of the subjects indicated that the goal of the task was to “match your own breathing to the audio signal”, suggesting that they paid more attention to the breathing and not the visual stimuli. Furthermore, several subjects reported difficulty viewing pleasant images during fast breathing, and that “pictures were more clear” during slow breathing epochs.

AUTONOMIC MEASURES

Each subject’s heart rate was averaged across each slow and fast breathing epoch in order to examine the effect of controlled breathing rate on heart rate. The mean heart rate across subjects was significantly lower during slow compared to fast breathing epochs (mean ± SEM: 60.96±0.36 beats/min (slow), 62.14±0.36 beats/min (fast), $p<0.01$, $t=3.39$).

Likewise, $EtCO_2$ values during each slow and fast breathing epoch were averaged to examine the effect of breathing rate on $EtCO_2$. Averaged across all subjects, these levels were significantly lower during fast compared to slow breathing epochs (mean ± SEM: 38±0.97mmHg (slow), 32±0.97mmHg (fast), $p<0.01$, $t=6.99$). However, $EtCO_2$ did not correlate ($r=-0.17$, $p = 0.538$) with heart rate across subjects. It is also important to note that $EtCO_2$ levels were not different between epochs in which positive or negative pictures were presented during slow (mean ± SEM: 37.1±1.13mmHg (pleasant); 37.6±1.13mmHg, (unpleasant), $t(14)=0.956$; $p=0.355$) or during fast (32.6±0.81mmHg (pleasant), 32.2±0.81mmHg (unpleasant), $t(14)=0.008$; $p=0.994$) breathing epochs; in other words, the BOLD activation differences could not be ascribed to CO_2 differences.

FUNCTIONAL IMAGING RESULTS

We examined activation within anterior cingulate and insular cortices during passive viewing of all positive versus all negative images, i.e., averaging across all fast and slow breathing epochs combined. Increased activation was observed in the left anterior insula (XYZ: -40/4/14, 384 mm^3, $t(15)=3.5$) while subjects passively viewed positive versus negative images and within right anterior cingulate cortex (XYZ:7/29/22, 320 mm^3, $t(15)=-2.6$) when subjects passively viewed negative versus positive images (**Figure 6S**).

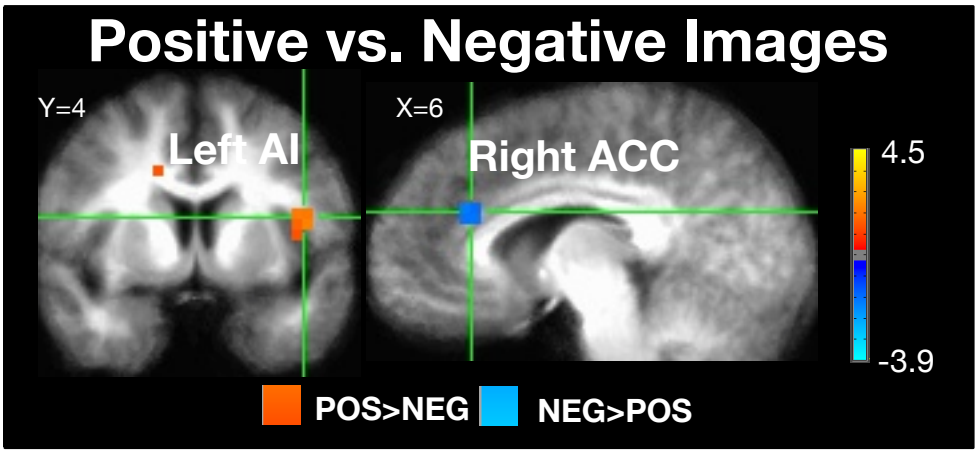

Figure 6S: **Positive vs. Negative Images (Fast and Slow Breathing combined)**. Increased LAI during positive and increased RACC during negative images was observed. Right=Left, Cf. text for details.

REFERENCES

1. Bauernfeind AL, de Sousa AA, Avasthi T, Dobson SD, Raghanti MA, Lewandowski AH, et al. A volumetric comparison of the insular cortex and its subregions in primates. J Hum Evol. 2013;64(4):263-79.
2. Craig AD. How do you feel?: an interoceptive moment with your neurobiological self: Princeton University Press; 2015.
3. Ito S, Craig AD. Vagal-evoked activity in the parafascicular nucleus of the primate thalamus. J Neurophysiol. 2005;94(4):2976-82.
4. Sovik R. The science of breathing--the yogic view. ProgBrain Res. 2000;122:491-505.
5. Tarvainen MP, Niskanen JP, Lipponen JA, Ranta-Aho PO, Karjalainen PA. Kubios HRV--heart rate variability analysis software. Comput Methods Programs Biomed. 2014;113(1):210-20.
6. Malik Mwc. Heart rate variability: standards of measurement, physiological interpretation and clinical use. Task Force of the European Society of Cardiology and the North American Society of Pacing and Electrophysiology. Circulation. 1996;93(5):1043-65.
7. Cox RW. AFNI: software for analysis and visualization of functional magnetic resonance neuroimages. ComputBiomedRes. 1996;29(3):162-73.
8. Talairach J, Tournoux P. Co-planar stereotaxic atlas of the human brain. New York: Thieme; 1988.
9. Forman SD, Cohen JD, Fitzgerald M, Eddy WF, Mintun MA, Noll DC. Improved assessment of significant activation in functional magnetic resonance imaging (fMRI): use of a cluster-size threshold. Magn ResonMed. 1995;33(5):636-47.